High-resolution mass spectrometric analysis of secondary organic aerosol produced by ozonation of limonene†

Maggie L. Walser,[a] Yury Desyaterik,[b] Julia Laskin,[c] Alexander Laskin[b] and Sergey A. Nizkorodov*[a]

Received 16th August 2007, Accepted 15th November 2007
First published as an Advance Article on the web 10th December 2007
DOI: 10.1039/b712620d

Chemical composition of secondary organic aerosol (SOA) formed from the ozone-initiated oxidation of limonene is characterized by high-resolution electrospray ionization mass spectrometry in both positive and negative ion modes. The mass spectra reveal a large number of both monomeric ($m/z < 300$) and oligomeric ($m/z > 300$) condensed products of oxidation. A combination of high resolving power ($m/\Delta m \sim 60\,000$) and Kendrick mass defect analysis makes it possible to unambiguously determine the molecular composition of hundreds of individual compounds in SOA samples. Van Krevelen analysis shows that the SOA compounds are heavily oxidized, with average O : C ratios of 0.43 and 0.50 determined from the positive and negative ion mode spectra, respectively. A possible reaction mechanism for the formation of the first generation SOA molecular components is considered. The discussed mechanism includes known isomerization and addition reactions of the carbonyl oxide intermediates generated during the ozonation of limonene. In addition, it includes isomerization and decomposition pathways for alkoxy radicals resulting from unimolecular decomposition of carbonyl oxides that have been disregarded by previous studies. The isomerization reactions yield numerous products with a progressively increasing number of alcohol and carbonyl groups, whereas C–C bond scission reactions in alkoxy radicals shorten the carbon chain. Together these reactions yield a large number of isomeric products with broadly distributed masses. A qualitative agreement is found between the number and degree of oxidation of the predicted and measured reaction products in the monomer product range.

Introduction

Atmospheric aerosols impact local air quality and human health, and play a large, as yet undetermined, role in controlling global climate.[1–6] A large portion of aerosol in both the free and polluted troposphere contains organic material, therefore it is important to understand the chemical composition and physical properties of the most representative types of organic aerosol constituents.[7–16] Increasingly sophisticated methods, such as high-resolution mass spectrometry, are used to determine the molecular composition of atmospherically relevant organic aerosol species.[17–21]

Condensed organic material resulting from the oxidation of volatile organic compounds (VOC) is usually found in secondary organic aerosol (SOA). Monoterpenes constitute a significant amount of biogenic VOC emissions and have been shown to form SOA in high yields.[22] The ability of monoterpenes to form SOA was recognized in 1960,[23] and has since been an area of great research interest. For many monoterpenes, SOA yields have been measured under different conditions, and the primary chemical components of SOA characterized by mass spectrometry and chromatography techniques. A variety of polyfunctional species, ranging from alcohols to ketones, aldehydes, and carboxylic acids have been detected among the gas- and particle-phase oxidation products.[24–26]

In the case of the ozone-initiated oxidation of D-limonene, Leungsakul *et al.*[24] recently described a semi-empirical mechanism that correctly reproduced the major first-generation products identified in SOA by chromatographic techniques. Limononaldehyde was the major identified product, followed by keto-limonene, keto-limononaldehyde, limononic acid, and keto-limononic acid (the corresponding structures are shown in Table 1). These products accounted for about 60% of the observed particle mass. Major gas-phase products included formaldehyde and keto-limonene.[25,26] A relatively stable endo-ozonide was also identified amongst the products.[26–28] Yields of SOA resulting from the ozonation of limonene were

[a] *Department of Chemistry, University of California Irvine, Irvine, California 92617-2025, USA. E-mail: nikorod@uci.edu; Fax: +1-949-824-8571; Tel: +1-949-824-1262*
[b] *Environmental Molecular Sciences Laboratory, Pacific Northwest National Laboratory, Richland, Washington 99354, USA*
[c] *Chemical and Materials Sciences Division, Pacific Northwest National Laboratory, Richland, Washington, 99354, USA*

† Electronic supplementary material (ESM) available: (a) Spreadsheets with m/z, relative abundances, and proposed elemental composition of all peaks in the positive and negative ion modes used for analysis (>0.5% relative intensity); (b) a large image containing a subset of all possible isomerization and decomposition pathways following decomposition of the initial endo-Criegee intermediates. Examples of stable products formed in this mechanism are outlined in Fig. 4–7, and are used to calculate the predicted properties of SOA species in Fig. 8. See DOI: 10.1039/b712620d

Table 1 Elemental composition for the 5 most abundant peaks observed in the positive (top) and negative (bottom) ESI ion modes. Up to 3 structures consistent with the measured compositions are shown in the last column. The structures are taken from the mechanism presented in Fig. 4–7 and in the ESM†

Measured m/z	Relative abundance	Ion composition	Non-ionized composition	Possible structures
209.0777	100	$NaC_9H_{14}O_4^+$	$C_9H_{14}O_4$	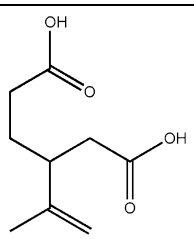 Limonic Acid 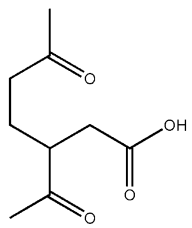 Keto-Limononic Acid 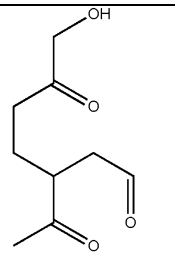 Keto-7OH-Limononaldehyde
207.0984	87	$NaC_{10}H_{16}O_3^+$	$C_{10}H_{16}O_3$	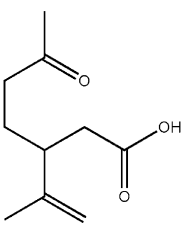 Limononic Acid 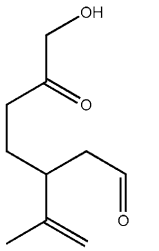 7OH-Limononaldehyde 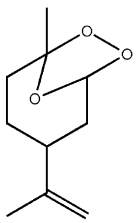 Endo-ozonide
223.0933	78	$NaC_{10}H_{16}O_4^+$	$C_{10}H_{16}O_4$	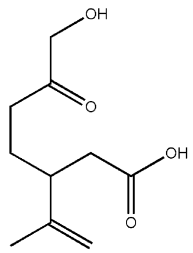 7OH-Limononic Aicd 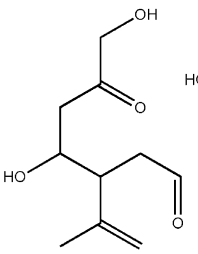 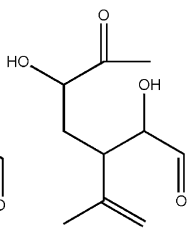
193.0827	51	$NaC_9H_{14}O_3^+$	$C_9H_{14}O_3$	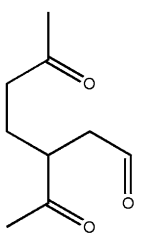 Keto-Limonaldehyde 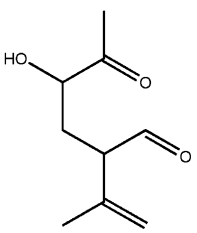 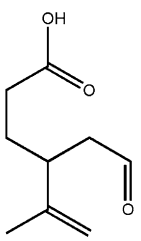 Limonalic Acid
191.1036	37	$NaC_{10}H_{16}O_2^+$	$C_{10}H_{16}O_2$	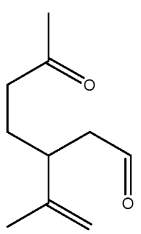 Limononaldehyde
185.0817	100	$C_9H_{13}O_4^-$	$C_9H_{14}O_4$	Same as for positive ion mode, m/z 209.0777
199.0974	37	$C_{10}H_{15}O_4^-$	$C_{10}H_{16}O_4$	Same as for positive ion mode, m/z 223.0933

 This journal is © the Owner Societies 2008

Table 1 (*continued*)

Measured *m/z*	Relative abundance	Ion composition	Non-ionized composition	Possible structures
171.0661	32	$C_8H_{11}O_4^-$	$C_8H_{12}O_4$	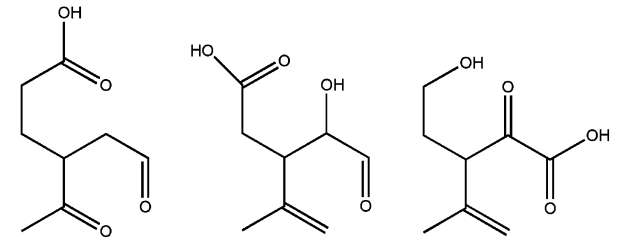 Keto-limonalic Acid
201.0766	25	$C_9H_{13}O_5^-$	$C_9H_{14}O_5$	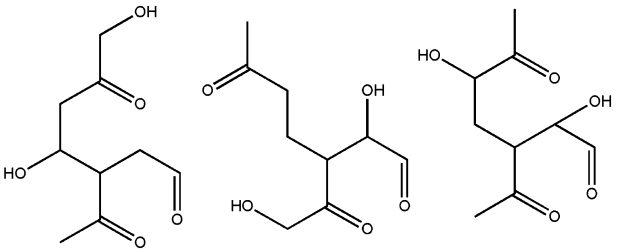
183.1024	17	$C_{10}H_{15}O_3^-$	$C_{10}H_{16}O_3$	Same as for positive ion mode *m/z* 207.0984

reported in ref. 29–33. The observed SOA yields for limonene are generally higher[29] than those for monoterpenes containing a single double bond, such as α- or β-pinene.

The presence of oligomeric species in terpene-derived SOA particles has been reported by multiple groups[19,34–42] but the mechanism of their formation is still not fully understood. This work focuses on the identification of the monomeric and oligomeric chemical species present in SOA particles produced from the ozone-induced oxidation of limonene. We take advantage of the rapidly developing tools of high-resolution mass spectrometry that have the potential to analyze aerosol particle composition without chromatographic separation techniques. Furthermore this work, along with that of Reinhardt *et al.*,[19] represents the first application of advanced mass spectrometric techniques developed for the analysis of complex mixtures to SOA characterization.

Typical mixing ratios of ozone in the lower atmosphere range from about 0.03 ppm (parts per million by volume) in clean air to over 0.3 ppm in heavily polluted air.[2] Atmospheric mixing ratios of monoterpenes rarely exceed 0.01 ppm. The mixing ratios of reactants used in this work are in the 1–10 ppm range, considerably higher than typical ambient levels. However, such high concentrations of ozone and limonene do occur in indoor air during building disinfection by ozone-generating air purifiers and normal cleaning, respectively.[43,44] Reactions between ozone and terpenes are well known to produce organic aerosol in indoor environments,[30,45–48] and the reaction products are known to be strong irritants.[49–51] An additional objective of this work is to provide information on the types of chemical functional groups, and the degree of oxidation, in aerosol constituents formed under such extreme oxidation conditions.

Experiment

Model SOA particles were formed by the ozone-initiated oxidation of D-limonene vapor in an inflatable Teflon reaction chamber (Fig. 1). A fan was used to ensure rapid mixing of ozone and limonene in the chamber. The chamber was first filled with approximately 200 L of oxygen (99.994% purity). Ozone was produced at concentrations ranging from 1–10 ppm using a small commercial ozone-generator (EZ-Com air purifier; 68 mg O_3 per hour[52]) placed directly inside the chamber. Pure oxygen was used rather than air to minimize impurities and avoid production of NO_x by the ozone source. Once the desired ozone concentration was achieved, a 0.1 slpm (standard liters per minute) oxygen flow saturated with D-limonene vapor was injected into the chamber over the

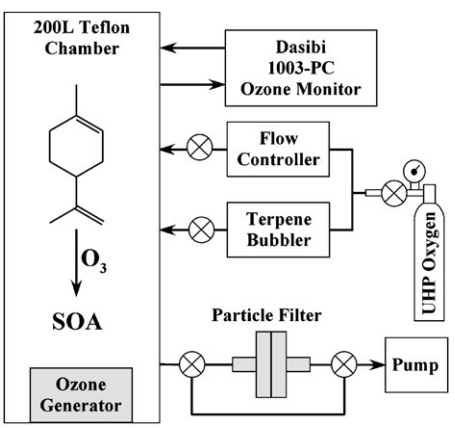

Fig. 1 Aerosol generation setup. Limonene reacts with ozone in the dark for 15–60 min. The aerosol samples are collected by filtration and extracted in a suitable solvent for mass spectrometric analysis.

course of 10 min. The saturated vapor was obtained by flowing oxygen through a temperature-controlled bubbler containing limonene (97% purity, Fisher Scientific) at $T = 298$ K (partial pressure of D-limonene = 260 Pa). In the absence of ozone, the final concentration of D-limonene in the 200 L chamber would be ~10 ppm, but this level was not achieved because oxidation and particle growth occurred in parallel with the slow D-limonene addition. The resulting mixture was allowed to age in the dark, at room temperature (~298 K), low relative humidity (~0–1%), and ambient pressure (~750 Torr), for 15–60 min before particle collection.

The particles were collected on a glass fiber filter by pumping air through the filter at 30 slpm over the course of ~6 min. The particle filter collection efficiency was >95% for particles larger than 0.1 μm.[53] The SOA material was subsequently extracted by sonicating the filter in 10 mL of solvent (methanol, acetonitrile, dichloromethane, or water). Secondary extraction of previously extracted filters resulted in much weaker mass spectra, suggesting that most soluble SOA material was extracted. It is possible, however, that a fraction of SOA material was not soluble in these solvents and remained on the filters. Isotopically labeled CD_3CN and CD_3OH solvents were used to assess the degree of functionalization of the analyte molecules by the solvents. Exposure to ambient light was minimized during the collection and extraction processes. The resulting extracts were then filtered through a 0.45 μm pore syringe filter before mass spectrometric analysis.

The composition of the SOA extracts was probed using a Finnigan LTQ (linear ion trap) Orbitrap™ Hybrid Mass Spectrometer (Thermo Electron Corporation) with a modified electrospray ionization (ESI) source. Samples were injected through a pulled fused silica capillary tip (50 μm id) at a flow rate of 0.5–1.5 μL min^{-1} using a spray voltage of 3.5 kV. The mass spectra were acquired in both positive and negative ion modes with a resolving power of 60 000 ($m/\Delta m$ at 400 amu). The instrument was calibrated using a mixture of stock solutions of caffeine, MRFA, and Ultramark 1621.

Results

High-resolution mass spectrometric data were used to generate the stick spectra shown in Fig. 2. Peaks resulting from solvent impurities were not included in the stick spectra. Fig. 2a shows a representative mass spectrum of a limonene-derived SOA sample extracted in acetonitrile obtained in the positive ESI ion mode with resolving power of 60 000. The spectrum contains more than 600 peaks in the m/z range of 100–1000 with intensities exceeding 0.5% of the most abundant peak at m/z 209.0777. The peaks are clustered in clearly identifiable groups separated by ~14 amu. In addition, there is a broader pattern resulting from the presence of oligomerization products: the cluster of peaks centered at m/z 200 corresponds to monomeric products; peaks centered at m/z 400 are dimeric products; and so on.

Composition of the observed peaks was determined by the mass spectrometer software (Xcalibur™) assuming that ions contain only ^{12}C, ^{13}C, ^{1}H, ^{16}O, and ^{23}Na atoms, and verified for consistency as described below. Analysis of the measured m/z values showed that all major positive peaks in the monomeric range ($m/z < 300$) contain one Na atom. Alternative composition assignments containing zero or two Na atoms resulted in deviations between the measured and predicted m/z values that were in excess of the experimental uncertainty. Therefore, complexation to $^{23}Na^+$ (m/z 22.9898) was assumed to be the primary ionization pathway for all positive peaks. This assumption is consistent with mass spectra of several standards recorded under similar experimental conditions.

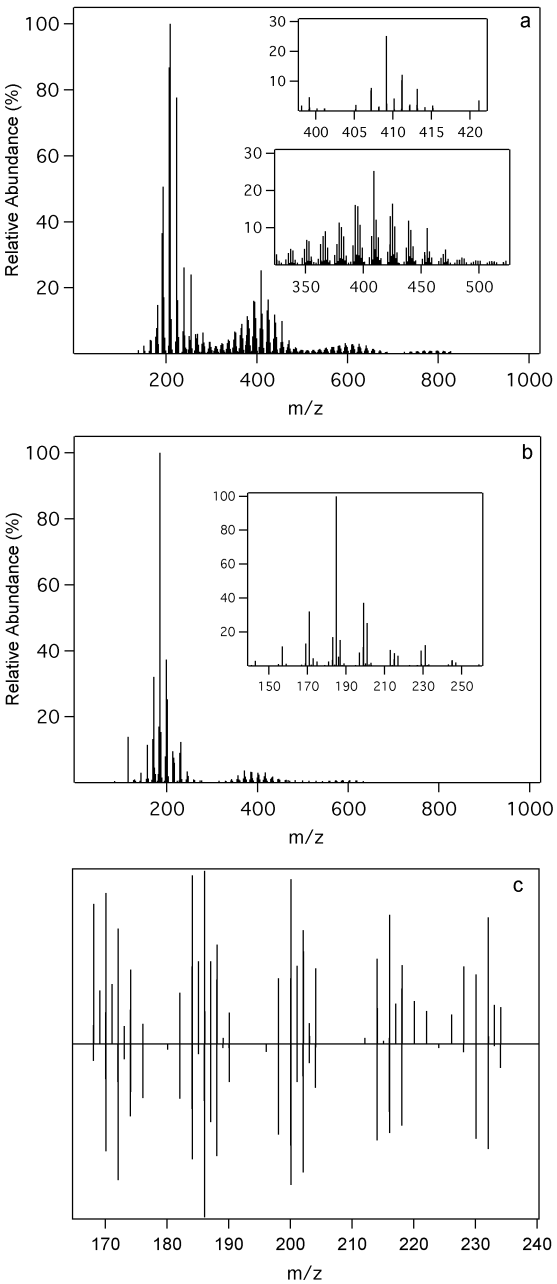

Fig. 2 Representative ESI mass spectra of SOA particles extracted in acetonitrile. The data include peaks with ≥ 0.5% abundance relative to the largest peak in the spectrum. (a) Stick spectra in the positive and (b) negative ion modes. (c) Comparison of positive (up) and negative (down) mass spectra on a logarithmic intensity scale after subtracting the exact mass of ^{23}Na from the positive m/z scale and adding the exact mass of ^{1}H to the negative m/z scale (to make the plot pertinent to the neutral analyte).

This journal is © the Owner Societies 2008

The mass spectrum of the same acetonitrile SOA extract obtained in the negative ESI ion mode is shown in Fig. 2b. It contains about 220 peaks above the 0.5% intensity threshold. The spectrum obtained in the negative mode displays very similar features to the positive-ion spectrum, *i.e.* broad features corresponding to monomeric, dimeric, and trimeric products as well as repeated clusters of peaks separated by $\sim$14 amu. Based on the mass spectra of standards, the major ionization pathway is deprotonation, *i.e.*, removal of a proton (m/z 1.0078) from the analyte molecules. Therefore, the composition was assigned assuming that the negative ions contain only ^{12}C, ^{13}C, ^{1}H, and ^{16}O atoms. There was no evidence for the presence of multiply charged ions ($z > 1$) in either positive or negative ion mode spectra.

The most abundant peaks in the positive and negative ion mode spectra, at m/z 209.0777 and 185.0817, respectively, were assigned to the same neutral precursor $C_9H_{14}O_4$, which most likely corresponds to limonic acid.[24] This is not an isolated coincidence. Table 1 shows elemental composition and possible structural assignments for the 5 most abundant peaks measured in each ion mode. All of these species are simultaneously detected in both modes. Furthermore, there is a good correlation between the positions and intensities of $[M + Na]^+$ peaks in the positive ion mode spectrum and $[M-H]^-$ peaks in the negative ion mode spectrum. To emphasize this point, Fig. 2c explicitly compares the positive ion mode spectrum shifted by the exact mass of one ^{23}Na atom and the negative ion mode spectrum shifted towards higher masses by the exact mass of the proton. The horizontal axis in this plot essentially corresponds to the molecular weight of the neutral analyte molecules. Although many peaks appear in both modes, there is also a significant number of peaks observed in only one ion mode, which indicates that data from both ion modes provide complementary information necessary for detailed characterization of the aerosol composition.

The spectra shown in Fig. 2 correspond to SOA prepared by reacting 10 ppm ozone and 10 ppm limonene for 1 h. Spectra were also obtained at different limonene : ozone ratios (10 ppm : 1 ppm and 1 ppm : 10 ppm) and at variable reaction times. SOA samples prepared using lower concentrations were all extracted in methanol and compared to the methanol analogs of the spectra shown in Fig. 2. A surprising result was that these spectra all had a similar overall appearance suggesting that the effect of reactants' concentrations on the distribution of extractable products is small. A considerably larger reaction chamber will be used in future experiments to obtain mass spectra at sub-ppm concentrations of reactants.

In addition, the reaction conditions were modified to include an excess amount of an OH-scavenger (up to 500 ppm of 2-butanol). Addition of the scavenger did not significantly affect the resulting mass spectra, suggesting that enough volatile products were generated by the oxidation of limonene to efficiently convert OH radicals produced by decomposition of carbonyl oxides into HO_2.

Mass spectra of SOA extracts in methanol looked qualitatively similar to the spectra of acetonitrile extracts, and the observed abundances of different features were comparable for both solvents. However, the exact peak positions were not identical, with clear evidence of methylation (addition of CH_3OH) of a large fraction of SOA peaks in the methanol mass-spectra. Indeed, for 51 and 45% of peaks below m/z 300 in the positive and negative ion modes, respectively, there is an overlap between peaks in acetonitrile mass spectra and peaks in the methanol mass spectra shifted down by 32.0262 amu, the molecular weight of a methanol molecule. The methylation was observed in both positive and negative ion modes suggesting that it occurred during the SOA extraction, and not during the electrospray process. MS/MS fragmentation experiments (not shown here) confirmed that methanol addition results in formation of new covalent bonds, rather than weakly associated complexes between ions and solvent molecules.

Additional evidence of solvent reactions was obtained using isotopically labeled solvents. There was no observable difference between positive ion mode spectra obtained from samples extracted in acetonitrile and acetonitrile-d_3, while negative ion mode spectra showed very few, likely insignificant, differences. These results indicate that acetonitrile does not react with analyte molecules. SOA samples were also extracted in both methanol and methanol-d_3. A comparison of the major peaks in the positive mode and smaller peaks in the negative ion mode showed a shift of 3.0188 amu, which corresponds to replacing 3 hydrogen atoms with 3 deuterium atoms when methanol solvent molecules react with analyte molecules. Detailed discussion of the effect of solvent on the analysis of SOA using ESI-MS will be presented in a separate publication.

Mass spectra obtained from dichloromethane SOA extracts were similar in the overall appearance but considerably weaker in intensity suggesting that the majority of the observed peaks correspond to moderately polar species. In addition, there were impurity peaks resulting from reaction between dichloromethane and ion source components. Spectra obtained for SOA samples extracted in water were comparable in both appearance and intensities to acetonitrile spectra obtained in the positive ion mode. In contrast, negative ion mode spectra were characterized by considerably weaker signal intensities. Therefore, dichloromethane and water were abandoned as SOA extracting solvents after a few initial trials. To avoid complications arising from solvent effects, the analysis described below is limited to mass spectra obtained using acetonitrile as the extracting solvent.

Two representative mass spectra recorded in acetonitrile were selected for a detailed analysis. All peaks in the negative ion mode above the 0.5% intensity cutoff were assigned a tentative elemental composition by Xcalibur™ assuming that the peaks contain only ^{12}C, ^{13}C, ^{16}O, and ^{1}H isotopes. We explicitly verified that all major peaks in the spectra had a neighboring peak at m/z + 1.0034 corresponding to incorporation of one ^{13}C atom. The ratio of intensities of ^{13}C- and ^{12}C-containing peaks was close to the expected $n_C \times 0.0108$, where n_C is the number of carbon atoms in the molecules. Although these ^{13}C peaks did not add additional information about SOA composition, they were used to confirm the validity of the peak assignments. In the positive ion spectra, the peaks were assumed to contain one ^{23}Na atom in addition to ^{12}C, ^{13}C, ^{16}O, and ^{1}H.

Because some of the elemental compositions suggested by Xcalibur™ had unrealistic C : H or C : O ratios, the initial peak assignments were additionally assessed for consistency using

Kendrick analysis.[54] This approach provides an effective visual method of presenting a mass spectrum in a two-dimensional way, and offers much more chemical insight into the composition of complicated mixtures than a standard mass spectrum. It introduces a new mass scale alternative to the ^{12}C-based IUPAC scale. The new mass scale can be based on any chemical moiety; CH_2 and oxygen atom are the most commonly used bases for the Kendrick analysis of complex mass spectra.[54] We illustrate this approach using a CH_2-Kendrick diagram that eliminates any mass defect due to the $^{12}CH_2$ group as an example. The Kendrick mass (KM_{CH_2}) is calculated by re-normalizing the IUPAC scale to the CH_2 Kendrick scale that equates the exact mass of the $^{12}CH_2$ group to 14.0000 amu (eqn (1)). The Kendrick mass defect (KMD) is calculated as the difference between the nominal value of KM (rounded up to the nearest integer) and KM (eqn (2)).

$$\mathrm{KM}_{\mathrm{CH_2}} = (m/z) \times \frac{14.000\ 00}{14.015\ 65} \quad (1)$$

$$\mathrm{KMD}_{\mathrm{CH_2}} = \mathrm{Nominal\,mass} - \mathrm{KM}_{\mathrm{CH_2}} \quad (2)$$

Kendrick plots are constructed by plotting the values of KMD_{CH_2} *vs.* KM_{CH_2}. The advantage of this approach is that KMD_{CH_2} values are identical for families of species that differ from each other only by the number of CH_2 groups, referred to hereafter as CH_2-families. Kendrick diagrams have been extensively used in petroleomics research,[55–57] and for the analysis of complex mass spectra of natural organic matter.[58–60] They have only recently been applied to the analysis of the chemical composition of organic aerosols.[19] The peaks were also analyzed by an analogous method in which the measured m/z values were normalized to a mass scale in which the m/z of the ^{16}O atom is 16.0000 amu (eqns (3) and (4)). To make our KMD_{CH_2} values directly comparable with the results of ref. 19 the nominal masses were calculated by rounding KM_{CH_2} up to the nearest integer; the same procedure was used for calculating nominal KM_O values.

$$\mathrm{KM}_{\mathrm{O}} = (m/z) \times \frac{16.000\ 00}{15.994\ 92} \quad (3)$$

$$\mathrm{KMD}_{\mathrm{O}} = \mathrm{Nominal\,mass} - \mathrm{KM}_{\mathrm{O}} \quad (4)$$

Fig. 3a shows a CH_2-Kendrick plot, *i.e.*, KMD_{CH_2} *vs.* KM_{CH_2}, constructed using the data from both the positive and negative mass spectra discussed earlier. For clarity, only data (including ^{13}C-containing peaks) above 1% relative abundance are shown. To make a meaningful comparison between positive and negative ion mode data, the KM_{CH_2} and KMD_{CH_2} values are calculated for the neutral precursors of the ions appearing in the ESI mass spectra. Specifically, because positive ions are cationized with sodium, $[M+Na]^+$, the m/z values measured in the positive ion mode have been shifted down by 22.9898 amu, and the m/z values of deprotonated $[M-H]^-$ ions measured in the negative ion mode have been shifted up by 1.0078 amu before calculating KM_{CH_2} and KMD_{CH_2}. The size of each point is proportional to the logarithm of the peak intensity. Fig. 3 also provides a visual representation of the degree of overlap between peaks measured in the two modes. For species observed in both negative and positive ion mode spectra, the experimental values of KMD are the same within the experimental uncertainty, $|\mathrm{KMD}^{(-)} - \mathrm{KMD}^{(+)}| < \sim 0.001$ amu.

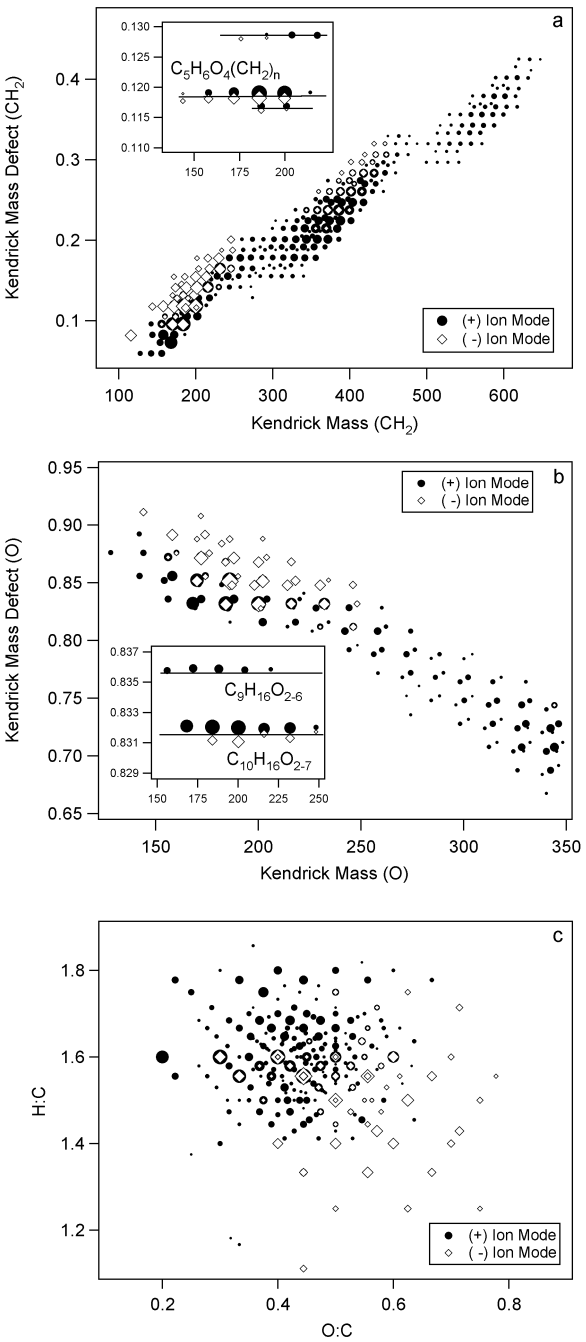

Fig. 3 Data with $\geq 1.0\%$ relative abundance, obtained in the positive and negative ion modes: (a) CH_2-Kendrick plot. Species separated by CH_2 groups fall on horizontal lines. (b) Oxygen Kendrick plot. Species separated by O atoms fall on horizontal lines. (c) van Krevelen plot. A plot of the H : C atomic ratio *versus* the O : C atomic ratio provides a visual representation of the degree of oxidation of the SOA component species. The size of the data points in all plots is proportional to the logarithm of the peak intensity. All plots are constructed for neutral species corresponding to ions detected in positive and negative mode mass spectra.

This journal is © the Owner Societies 2008

Table 2 Expected slopes of KMD_{CH_2} *vs.* KM_{CH_2} for several model polymers with a variable degree of oxidation

Family	Description	KMD_{CH_2}/KM_{CH_2}
$(CH_2)_n$	Polyethylene	0
$(C_2H_4O)_n$	Polyol: OH on every second C-atom	5.22×10^{-4}
$(CH_2O)_n$	Polyol: OH on every C-atom	7.65×10^{-4}
$(C_3H_4O)_n$	Polycarbonyl: O on every third C-atom	6.49×10^{-4}
$(C_2H_2O)_n$	Polycarbonyl: O on every second C-atom	8.66×10^{-4}
$(CO)_n$	Polycarbonyl: O on every C-atom	1.30×10^{-3}
CO_2	Carbon dioxide	1.35×10^{-3}

Points with identical KMD_{CH_2} forming lines parallel to the *x*-axis correspond to families of species $C_xH_yO_z(CH_2)_n$ with a fixed oxygen atom content (x, y, z = fixed; n = variable) and varying numbers of CH_2 groups. For example, one of the lines in the inset in Fig. 3a corresponds to a family $C_5H_6O_4(CH_2)_n$ with n ranging from 0 to 4 for negative ions and from 2 to 6 for positive ions. Average experimental values of KMD_{CH_2} for this family are 0.1183 (negative ions) and 0.1191 (positive ions), which is equal to the predicted KMD_{CH_2} of 0.1186 within the experimental error in m/z. For the data sets used in this analysis, such n-families generally contained up to 8 and 6 members in the positive and negative ion mode spectra, respectively.

For species containing only carbon, hydrogen, and oxygen, a larger CH_2-Kendrick defect generally implies a higher degree of oxidation. To illustrate this point, Table 2 shows expected values for the ratio of KMD_{CH_2} to KM_{CH_2} for several polymers and for CO_2. For our SOA samples, the observed magnitude of the KMD_{CH_2} increases with KM_{CH_2} with a slope of $\sim 7 \times 10^{-4}$, which is approaching a value characteristic of heavily oxidized polyethylene. There is also a slight downward shift in the slope between the monomer and dimer, and between the dimer and trimer, regions of the plot, indicating a decreasing O : C ratio with mass, which is also consistent with the reported results of mass spectrometric characterization of SOA produced from oxidation of α-pinene.[19]

Fig. 3b shows an oxygen Kendrick plot, in which the experimental m/z values have been normalized to the exact mass of the oxygen atom. In this plot, horizontal lines with identical KMD_O values correspond to families of species separated from each other only by the number of oxygen atoms: $C_xH_yO_m$ (x, y = fixed; m = variable). The inset in Fig. 3b shows two such O-families corresponding to $C_9H_{16}O_{2-6}$ (theoretical $KMD_O = 0.8353$) and $C_{10}H_{16}O_{2-7}$ (theoretical $KMD_O = 0.8315$). The observed values of m were surprisingly high, with addition of up to 7 oxygen atoms observed in the monomeric region ($m/z < 300$; Fig. 3b). This is consistent with a similar observation of highly oxidized species $C_{10}H_{16}O_5$ and $C_{10}H_{16}O_6$ in a previous mass-spectrometric study of the ozone-initiated oxidation of limonene.[17]

In addition to Kendrick analysis, the peak assignments were examined for self-consistency using the van Krevelen approach, which plots the atomic ratio of hydrogen to carbon *versus* the atomic ratio of oxygen to carbon (Fig. 3c).[61] Approximately 70% of the peaks have an O : C ratio between 0.4 and 0.6. Species with O : C ratios greater than 0.6 produce larger peaks in the negative mode, while species with O : C ratios smaller than 0.4 are more readily seen in the positive ion mode, reflecting much higher sensitivity for carboxylic acids in the negative ion mode. The average O : C ratios calculated using peak intensities as weighting factors are 0.43 and 0.50, determined from the positive and negative ion mode spectra, respectively. This corresponds to an impressively high degree of oxidation, wherein every second carbon atom is bonded to an oxygen atom.

Most peaks have an H : C ratio smaller than 1.6, which is the H : C ratio of limonene itself. However, a number of peaks with H : C in excess of 1.6 are also observed. Specifically, in the positive ion mode, 50% of peaks have an H : C ratio larger than 1.6, while in the negative ion mode, that percentage decreases to approximately 30%. The general properties of the plot agree with the recent analysis of α-pinene SOA.[19]

Assignments proposed by the Xcalibur™ software that resulted in obvious outliers on Kendrick and/or van Krevelen diagrams were re-assigned to an alternative atomic composition within ±0.001 m/z of the experimental peak position. Assignments were accepted only if they belonged to an existing CH2- or O- family on the Kendrick plots (Fig. 3a and 3b) and had physically meaningful H : C and O : C atomic ratios. A small number of peaks, generally less than 2% relative abundance, remained unassigned. These peaks are excluded from Fig. 3 and from the table of assigned peaks provided in the ESM.†

Discussion

The mass spectra discussed above contain a large number of peaks, well beyond the number of products described in previously reported studies of limonene ozonation.[24–28] Even with the benefit of knowledge of elemental compositions of every peak, it is close to impossible, not to mention impractical, to assign all peaks to specific molecular structures. However, one can test whether known chemistry of the ozonation of olefins is consistent with the large number of observed products, and whether it correctly predicts the C : O : H ratios in the SOA constituents.

In the following discussion, we assume that the first step in the oxidation of the limonene molecule involves an attack on its endocyclic double bond by ozone (Fig. 4). The rate constant for the reaction of ozone with the exocyclic double bond is estimated to be an order of magnitude smaller than for the endocyclic double bond.[24,33] Thus, the exocyclic double bonds are expected to be less reactive, and they are likely to react only when most of the endo bonds are consumed. A significant fraction of the exocyclic bond oxidation reactions is expected after the first-generation products condense in the aerosol phase, and not in the gas phase.[33] Note that these assumptions are not entirely accurate as products corresponding to the initial ozone attack on the exocyclic double bond in limonene have also been observed (*e.g.*, keto-limonene).[24,62] Furthermore, some of the observed products still contain the intact exo bond even under the excess ozone conditions, suggesting that burial of first generation products inside aerosol particles may protect them from further oxidation. However, the order in which the double bonds are oxidized and the degree

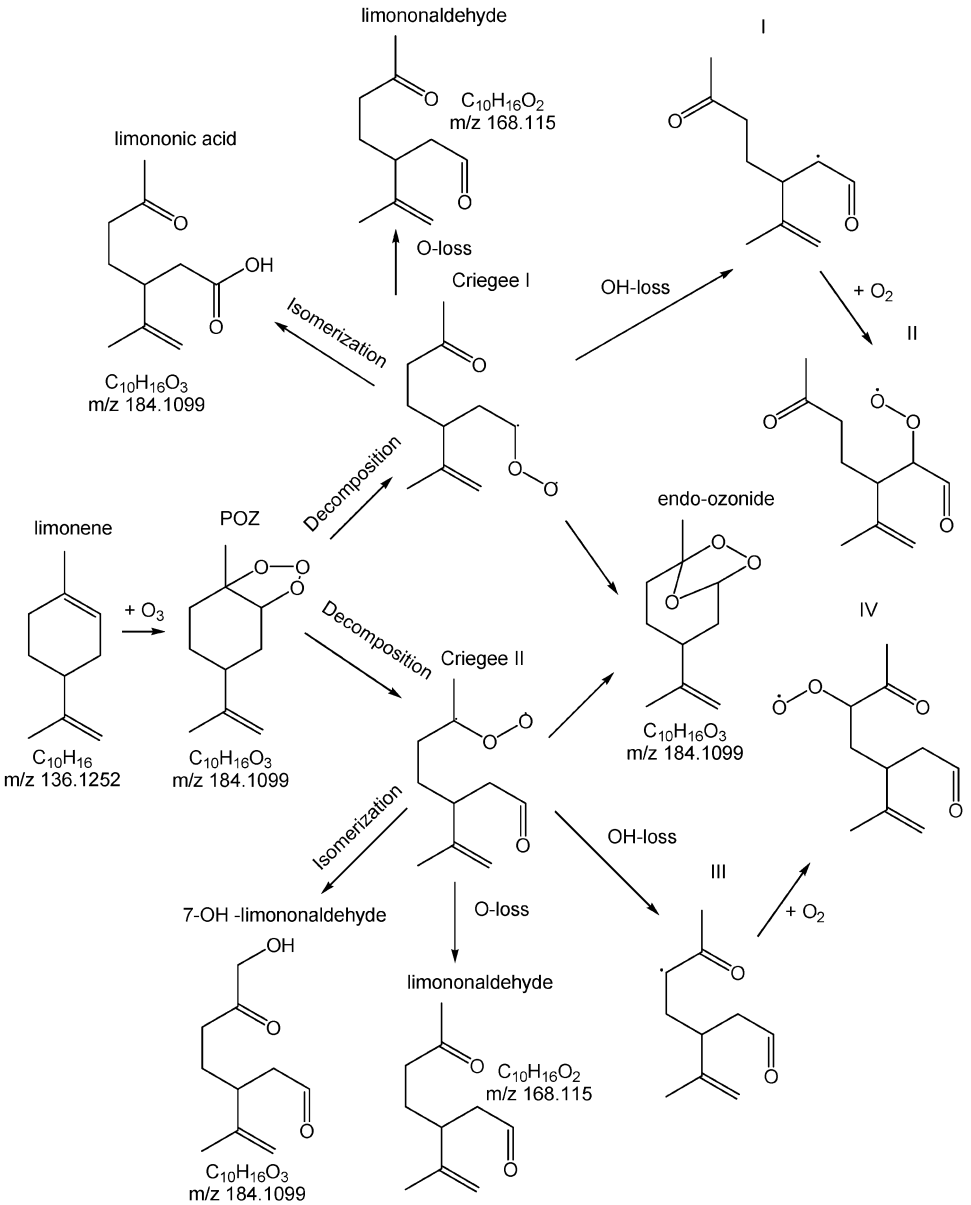

Fig. 4 Mechanism for primary product formation from oxidation of the endo-double bond. Radical species are marked with roman numerals, and stable products have names, formulas, and m/z values next to the structures. The initial process proceeds *via* the Criegee mechanism, and is followed by subsequent reactions involving the highly reactive Criegee intermediate.

of oxidation will not affect the overall conclusions of this analysis.

The initial ozone attack on the endocyclic double bond generates an unstable primary endo-ozonide (POZ) that quickly decomposes into one of two possible endo carbonyl oxides (labeled Criegee I and II in Fig. 4). These carbonyl oxides are endowed with a considerable amount of internal energy that is disposed of by isomerization, decomposition, or recombination, leading to a host of known products of the ozonation of limonene.[24–28] Fig. 4 shows pathways to previously identified products of ozonation of limonene including limononic acid, limononaldehyde, 7-OH-limononaldehyde, and the endo-ozonide.

The reaction mechanism up to this point can be regarded as well understood, as documented in previous studies.[24–28] However, the limited number of products (<10) expected from commonly considered limonene ozonation steps shown in Fig. 4 is clearly inconsistent with the complexity of the observed mass spectra. We propose that the critical step responsible for the large number of observed oxidation products is the decomposition of the carbonyl oxide into an OH radical and an alkyl radical R, *e.g.*, Criegee I decomposition into alkyl radical (I) in Fig. 4. Loss of OH from carbonyl oxides can be a very efficient process with the branching ratio for this channel approaching unity in certain cases.[63–65] Despite this large branching ratio, the fate of the organic radicals produced by decomposition of limonene carbonyl oxides has previously been disregarded.

Once the alkyl radical is generated, it immediately reacts with an oxygen molecule to become an alkylperoxy radical

 This journal is © the Owner Societies 2008

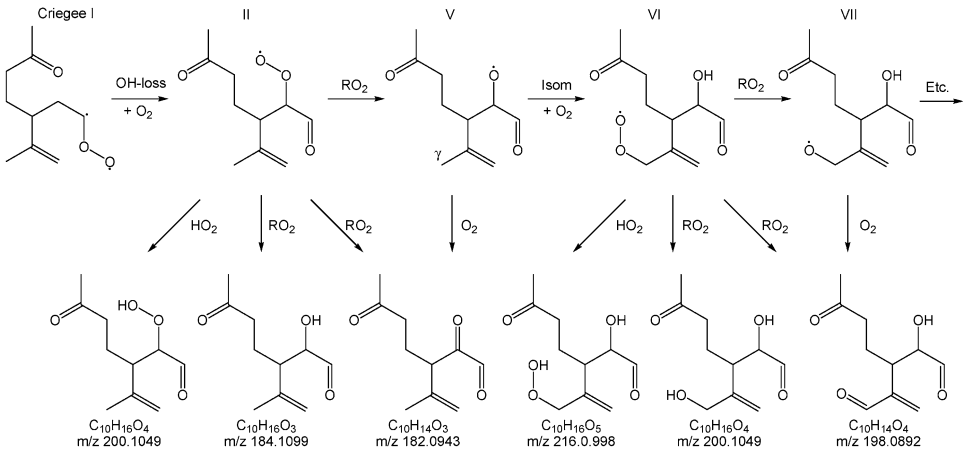

Fig. 5 A sample RO isomerization pathway resulting in species with a progressively increasing number of oxygen-bearing functional groups in the final products. Radical species are marked with roman numerals, and stable products have formulas and m/z values posted next to the structures.

RO_2, *e.g.*, (I) + O_2 → (II).[2] Under the NO_x free conditions of our experiment, the primary loss processes for RO_2 radicals are reactions with other $R'O_2$ radicals that proceed by several competing pathways (Fig. 5). The first pathway is a termination step that eliminates two free radicals and generates two stable products (eqn (5)). The second pathway is a propagation step that converts alkyl-peroxy radicals into much more reactive alkoxy radicals (eqn (6)). The relative importance of the first two pathways are comparable, with $k_5/(k_5 + k_6)$ values generally falling in the range of 0.4–0.7[66] indicating that alkoxy radicals (RO; *e.g.* v) can be produced with substantial yields. The formation of organic peroxides may occur in reactions of RO_2 with HO_2 (eqn (7)); it is negligible in RO_2 self-reactions.[66]

$$RO_2 + R'O_2 \rightarrow \text{alcohol} + \text{carbonyl} + O_2 \qquad (5)$$

$$RO_2 + R'O_2 \rightarrow RO + R'O + O_2 \qquad (6)$$

$$RO_2 + HO_2 \rightarrow ROOH + O_2 \qquad (7)$$

From this point, the RO radicals have three possible fates.[2,67] The most likely process is isomerization involving a facile intramolecular abstraction of a hydrogen atom from the γ-carbon atom (if one is available). Fig. 5 shows that isomerization of RO radical (v) immediately followed by addition of an oxygen molecule produces another RO_2 radical (vi) that now carries an alcohol group. Repeated RO_2 self-reactions ((5) and (6)) followed by RO isomerizations incorporate multiple oxygen atoms in the resulting products leading to the appearance of families of $C_xH_yO_m$ with values of m as high as 7, as Fig. 3b demonstrates.

Another possible fate for RO radicals is reaction with an oxygen molecule leading to formation of a stable carbonyl and HO_2 radical, which then reacts with RO_2 radicals *via* reaction (7) to generate organic peroxides. Finally, the RO radical (v) can decompose (Fig. 6) by scission of the bond between the alkoxy and α-carbon atoms, a process that generates a stable aldehyde and an alkyl radical (viii) that has fewer carbon atoms than the RO radical from which it originated. Such decomposition processes are known to be quite efficient, especially in oxygen-containing alkoxy radicals.[67] The alkyl radical will immediately add an oxygen molecule to form another RO_2 (ix). Repeated RO_2 self-reactions and bond scissions in the resulting RO radicals will lead to progressively smaller products. A combination of all these processes results in a very broad array of final products, each containing one or more –OH, –OOH, –CHO, –C(O)–, and/or –COOH functional groups.

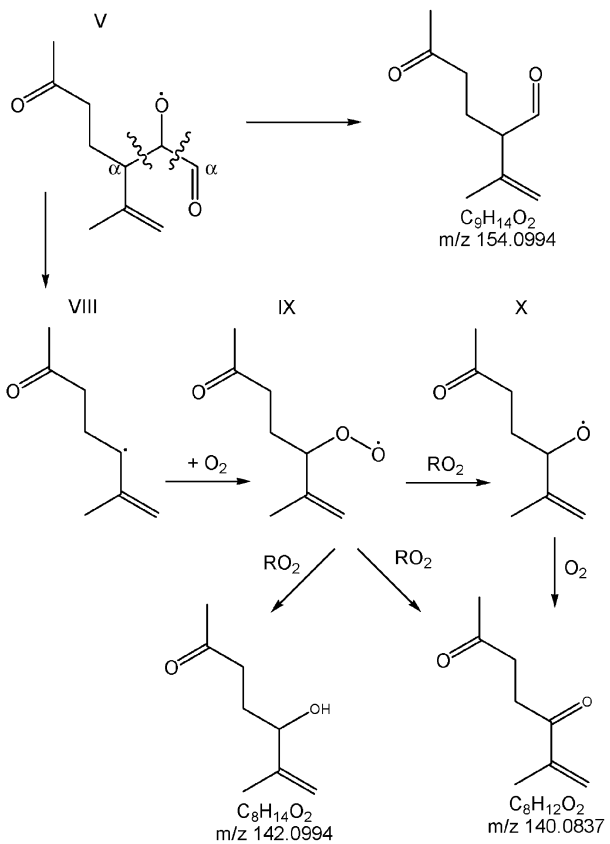

Fig. 6 A sample RO radical decomposition pathway. The bond scission between the alkoxy and α-carbons in RO radicals results in new RO radicals with fewer carbon atoms than in the parent molecule.

The main objective of this work is not to create a comprehensive list of all possible reactions that can conceivably take place during limonene ozonation, but to judiciously select a minimal set of the most likely chemical processes that would result in reaction products consistent with the observed mass spectra. To this end, the ESM † to this paper includes an image with a proposed set of initial reactions following the decomposition of endo-carbonyl oxides of limonene labeled Criegee I and Criegee II in Fig. 4. The fates of the resulting free radicals are traced for a fixed number of reaction steps tabulating all stable products that are formed along the way. Based on kinetics considerations, the number of successive $RO_2 \rightarrow RO$ conversions (6) in every reaction branch is limited to four, and no more than one C–C bond scission in RO radicals is allowed per reaction branch. RO isomerization is allowed to abstract H-atoms only from γ-carbon atoms. Free radicals containing fewer than six carbon atoms are not traced because they are not expected to result in condensable products. Secondary reactions initiated by the OH by-product of carbonyl oxide decomposition are neglected based on the lack of difference in the mass spectra of SOA generated in the presence or absence of an OH-scavenger (2-butanol). Oligomerization reactions and cross reactions between stable products are not considered in this manuscript either.

Even with these restrictive assumptions, the mechanism predicts a large number of monomeric products resulting from the chemistry of RO and RO_2 radicals. Indeed, nearly 90 stable products can be identified in the ESM diagram.† Each product contains on average 3–4 functional groups (–OH, –OOH, –HCO, –COOH, and/or –C(O)–), and many are structural isomers of each other, with an average of 2–3 isomers per predicted elemental composition.

Although inclusion of the processes shown in the ESM† certainly improves the agreement with the overall number of observed products, the masses and the degree of oxidation of the predicted products are not fully consistent with experimental data shown in Fig. 3. Therefore, secondary reactions involving oxidation of the exo-double bond in limonene have to be included. Indeed, almost all stable products formed in the reactions diagrammed in the ESM† still contain the intact exo-double bond, and can be represented by the general formula $R_1R_2C{=}CH_2$, where R_1 and R_2 are derived from limonene's ring and methyl group, respectively. As a result of alkoxy isomerization chemistry, R_2 can be transformed from $–CH_3$ (the initial group from limonene) to either –CHO, $–CH_2OH$, or $–CH_2OOH$. Classical Criegee oxidation of $R_1R_2C{=}CH_2$ produces a corresponding ketone $R_1R_2C{=}O$, thus increasing the mass of the original species by 1.9792 amu (Fig. 7a). Reaction (b) in Fig. 7 shows the loss of CO_2 from the exo-carbonyl oxide (R_1R_2COO) resulting in a stable product R_1–R_2, which is equivalent to the loss of C_2H_2 (26.0157 amu) from the original species. The exo-carbonyl oxide can also decompose to form an alkyl radical (R_1), followed by the immediate addition of an oxygen molecule to form an alkylperoxy radical (R_1O_2). The latter is converted into a carbonyl or alcohol with fewer carbons than the original species (Fig. 7c).

In addition to oxidation of the exo-double bond, aldehydes formed in the initial processes (*e.g.*, limononaldehyde) can be partly oxidized to carboxylic acids (Fig. 7d). Although oxidation of aldehydes by ozone is slow in the gas phase,[68] it should be faster inside aerosol particles. Even the small amount of carboxylic acids produced will result in a sizeable signal in the mass spectrum because of the exceptionally high ionization efficiency of carboxylic acids. Therefore, we assume that all molecules containing at least one aldehyde group may undergo partial oxidation (–CHO → –COOH) that increases the mass of the original aldehyde by 15.9949 amu.

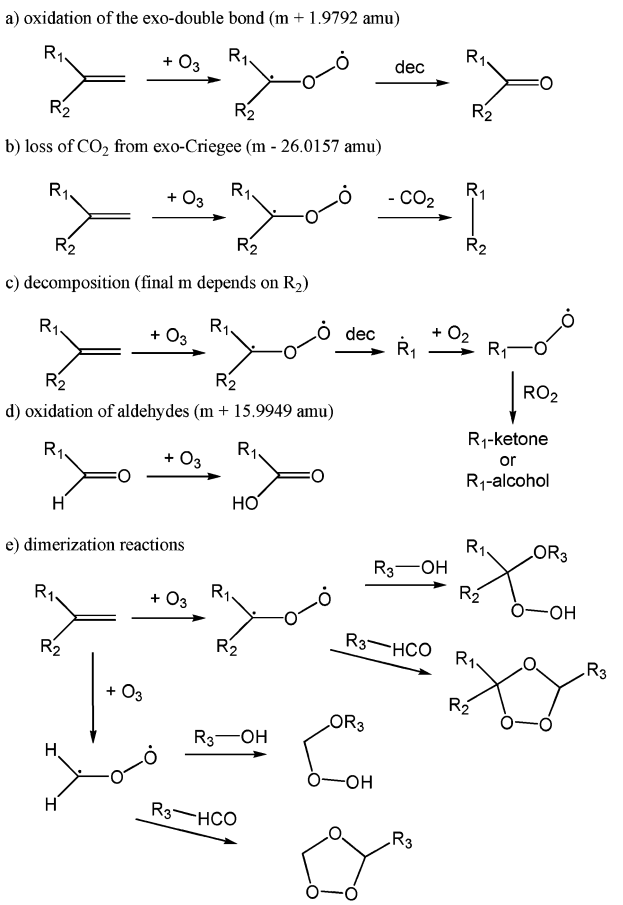

Fig. 7 Mechanism for secondary product formation resulting from the oxidation of the exo-double bond. Further oxidation of double bonds and aldehydes in primary products, as well as dimerization, leads to increased species complexity in the SOA.

Finally, Fig. 7e shows examples of possible condensation reactions that result in the formation of exo-ozonides and alkylperoxides. The only condensation processes included in this mechanism are reactions of the stabilized carbonyl oxide CH_2O_2. As oxidation of the exo-double bonds mostly occurs in the aerosol phase,[33,62] the degree of stabilization of carbonyl oxide CH_2O_2 should be significant, and it should add to available aldehydes, acids, and alcohols with high efficiency. For simplicity, we assume that each primary product may add no more than one CH_2O_2 unit as a result of these condensation reactions.

Formal, mechanistic application of processes in Fig. 7a–c to all first-generation products from the oxidation of the endo-double bond increases the number of possible products in the monomeric region to over 400. Inclusion of the aldehyde

 This journal is © the Owner Societies 2008

oxidation (Fig. 7d) and CH_2O_2 addition (Fig. 7e) further increases the number of products to over 1100. Many of these products are isomers with an identical elemental composition but different structures. Accounting for the structural isomerism and for identical species formed *via* different pathways, we still predict some 140 species with distinct atomic composition in the monomeric region. This prediction is consistent with the large number of peaks observed in the positive and negative ion mode mass spectra below m/z 300.

The SOA particles examined here were produced by oxidation of limonene in ultra-pure oxygen instead of air to avoid possible involvement of NO_x species and other impurities. The conversion from alkyl radicals (R) into alkyl peroxy radicals (RO_2) is not a rate limiting step,[2] and therefore it should not be affected by the O_2 concentration. The rates of RO + O_2 reactions are accelerated fivefold in pure oxygen. However, isomerization is expected to be the major reaction channel for most RO radicals involved in the mechanism. Therefore, we do not anticipate a drastic difference in the composition of aerosol particles generated in pure oxygen instead of dry air.

To verify whether the mechanism results in a correct degree of oxidation in the final products, Fig. 8 compares (a) the predicted KM_{CH_2} and KMD_{CH_2} values and (b) the predicted H : C *versus* O : C ratios with those measured using high-resolution mass spectrometry in both the positive and negative ion modes. Predicted m/z values correspond to exact masses of the first generation products (shown in the ESM diagram†), as well as the possible mass increases and decreases resulting from the subsequent reactions outlined in Fig. 7a–e. The experimental points plotted in Fig. 8 correspond to the experimental m/z values shifted down by the exact mass of ^{23}Na (22.9898 amu) for positive ions and m/z values observed in the negative ion mode shifted up by the mass of ^{1}H (1.0078). This allows direct comparison of neutral products rather than their corresponding ions.

Comparison of the predicted and measured mass defects gives credence to the qualitative validity of the presented mechanism. In addition to the good agreement between the number of observed and predicted peaks, the magnitudes of the mass defects are similar. The products predicted by the presented empirical model are on average smaller than observed. However, it is likely that the lower mass products predicted by our mechanism have a high enough vapor pressure that they exist in the gas phase rather than the aerosol phase under our experimental conditions. If this were the case, these lower-mass species would not have been detected, as we analyzed only those products that remained in the filtered SOA samples.

As discussed earlier, the Kendrick representation allows for the visual identification of homologous species separated by an integer number of O-atoms or –CH_2– groups. The existence of $C_xH_yO_m$ families with the same values of x and y and variable m (O-families) is relatively straightforward to account for by the consecutive RO isomerizations. To illustrate this point, consider the reaction sequence shown in Fig. 4. Alkyl peroxy radical (II) can react with HO_2 or RO_2 to generate a stable peroxide $C_{10}H_{16}O_4$, alcohol $C_{10}H_{16}O_3$ and carbonyl $C_{10}H_{14}O_3$. The radical reaction chain can be propagated instead to alkoxy radical (V), which can isomerize into the

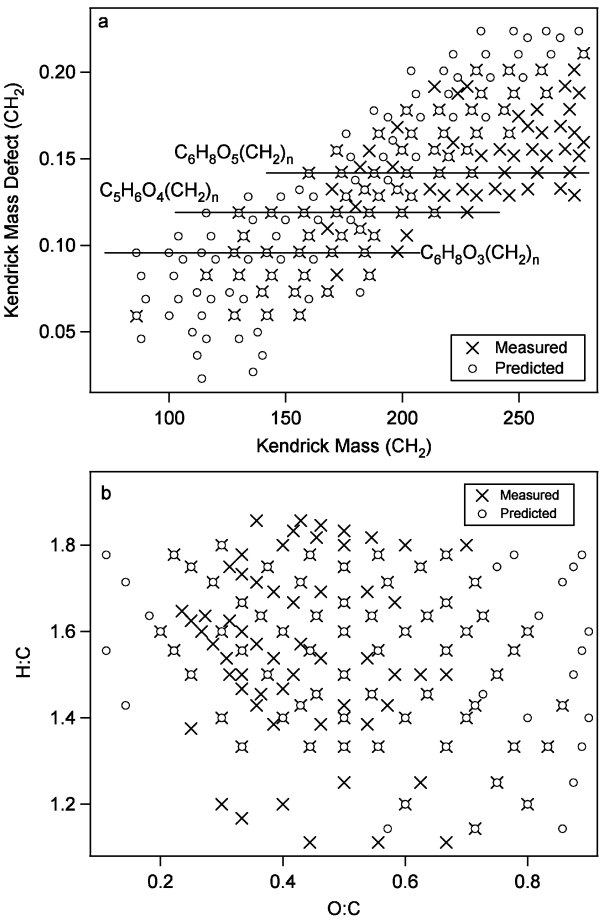

Fig. 8 Comparison of experimentally observed and predicted SOA species. (a) The CH_2-Kendrick plot is used to compare the experimental m/z values in both ion modes with the molecular weights of the products predicted by the oxidation mechanisms. (b) A van Krevelen diagram is used to compare the H : C and O : C ratios measured in both ion modes with the ratios predicted by our mechanism. All plots are constructed for neutral species corresponding to ions detected in positive and negative mode mass spectra. Open circles represent peaks predicted by the empirical reaction mechanism and crosses represent peaks measured in the positive and/or negative ion modes.

alkyl peroxy radical (VI). The latter generates a new set of products, peroxide $C_{10}H_{16}O_5$, alcohol $C_{10}H_{16}O_4$ and carbonyl $C_{10}H_{14}O_4$, which are different from the previous set by one oxygen atom. Repeated RO isomerizations followed by RO_2 self-reactions create families of products on the O-Kendrick plots containing a variable number of –OH functional groups. Certain secondary reactions, such as oxidation of aldehydes to acids (Fig. 7d), also contribute to the formation of O-families.

Fig. 8a shows that the proposed mechanism also generates families of $C_xH_yO_z(CH_2)_n$ species with fixed x, y, z and variable n. This is a curious observation given that the reaction mechanism does not include any direct CH_2 abstraction or insertion processes. However, scission reactions (Fig. 5) and/or exo-carbonyl oxide decomposition reactions (Fig. 7c) account for the appearance of such families. For example, scission of one of the C–C bonds in radical (V) shown in Fig. 6 directly produces a stable product with chemical

formula $C_9H_{14}O_2$. Scission of the second C–C bond in (v) results in alkyl peroxy radical (ix) that yields a stable product with formula $C_8H_{12}O_2$, which differs from the first stable species by one CH_2 unit.

In general, mechanistic understanding of the relationship between different members of CH_2-families is not as straightforward as for the members of O-families. It therefore follows that for the oxidation of monoterpenes, O-Kendrick representation of mass spectra is more informative than CH_2-Kendrick diagrams.

One would expect that oxidized limonene products should have H : C ratios that are smaller than 1.6, the H : C ratio of limonene itself. We find that a large number of products have an H : C ratio in excess of 1.6 (Fig. 3). A similar observation was made in the high-resolution mass-spectrometric analysis of SOA produced by ozonolysis of α-pinene, and attributed to unspecified secondary hydrogenation reactions.[19] Indeed, condensation reactions of the initial products with small molecules with H : C $>$ 1.6 (*e.g.* with formaldehyde or water) would increase the H : C ratio. However, Fig. 8b shows that the proposed mechanism generates products with H : C ratio $>$ 1.6 without invoking such hydrogenation processes. For example, the loss of CO_2 during decomposition of carbonyl oxides increases the H : C ratio. Additionally, formation of a stable alcohol through RO_2 self-reactions or peroxide through reaction of RO_2 with HO_2 results in addition of a hydrogen atom without addition of a carbon atom, which also increases the H : C ratio.

Fig. 8b also illustrates that a number of points in the O:C–H:C coordinate space remain unexplained by the assumed reactions of RO and RO_2 free radicals. This is likely a result of the over restrictive rules built into the presented mechanism (for example, the requirement for RO radicals to abstract H-atoms only from γ-carbon atoms). However, this may also reflect neglect of secondary chemistry taking place in the condensed phase. Cross-polymerization of carbonyls, decomposition of peroxides and ozonides, cyclization of molecules containing carbonyl and hydroxyl functional groups, ester formation, and similar processes may slowly change the composition of SOA samples as they are collected and analyzed. Therefore, our future efforts will be directed toward understanding the mechanism of slow aging processes in SOA.

Conclusions

High-resolution mass spectrometric characterization of SOA particles formed from the ozone-induced oxidation of limonene confirmed that the composition of these particles is significantly more complex than that predicted by the basic Criegee mechanism of alkene ozonolysis. This work convincingly demonstrates that in order to account for the very large number of poly-functional species that exist in SOA in both monomeric and polymeric form, one has to include rich chemistry involving alkylperoxy and alkoxy radicals formed from the decomposition of carbonyl oxide intermediates. Furthermore, we describe a minimal set of reactions required to produce a distribution of limonene ozonation products that is consistent with mass-spectrometric observations. Even with a fairly restrictive set of reaction rules, inclusion of alkylperoxy and alkoxy chemistry in limonene ozonation produces some 1000 products with 140 unique m/z values in the monomeric mass range ($m/z < 300$). The large number of isomeric products produced in the oxidation of just one terpene shows how challenging it will be to obtain detailed characterization of molecular composition of ambient SOA particles that typically result from oxidation of multiple precursors.

The ultimate goal of research on chemical mechanisms of SOA formation is to find out which reactions out of the infinite number of possibilities actually take place, and which are likely to be insignificant. We expect that for such complex systems the answer to this question will come from coupling mass spectrometry and information theory, and this work can be viewed as the first step in that direction.

We take advantage of both positive and negative ion mass spectra mode, which allows the identification of a more complete set of SOA species. The similarities and differences between spectra obtained in the two ion modes clearly show that complementary information is obtained by using both modes. Our analysis shows that more oxidized species (*e.g.* carboxylic acids *vs.* corresponding aldehydes) are more readily detected in the negative ion mode. The use of Kendrick and van Krevelen analysis, tools commonly used in mass spectrometry of complex mixtures, allows the identification of homologous series of products with varying degrees of oxidation. Analysis of oligomeric species ($m/z > 300$) is currently underway, and this, along with a proposed mechanism for oligomer formation, will be presented in another publication.

Acknowledgements

This study was supported by the National Science Foundation through the Environmental Molecular Science Institute program, grant CHE-0431312, and Atmospheric Chemistry program, grant ATM-0509248. M.L.W. was supported by a National Science Foundation Graduate Research Fellowship. The research described in this paper was performed in the Environmental Molecular Sciences Laboratory, a national scientific user facility sponsored by the Department of Energy's (DOE) Office of Biological and Environmental Research and located at the Pacific Northwest National Laboratory. J.L. acknowledges support from the Chemical Sciences Division, Office of Basic Energy Sciences of the US DOE.

References

1 M. Kanakidou, J. H. Seinfeld, S. N. Pandis, I. Barnes, F. J. Dentener, M. C. Facchini, R. Van Dingenen, B. Ervens, A. Nenes, C. J. Nielsen, E. Swietlicki, J. P. Putaud, Y. Balkanski, S. Fuzzi, J. Horth, G. K. Moortgat, R. Winterhalter, C. E. L. Myhre, K. Tsigaridis, E. Vignati, E. G. Stephanou and J. Wilson, Organic aerosol and global climate modeling: A review, *Atmos. Chem. Phys.*, 2005, **5**, 1053–1123.

2 B. J. Finlayson-Pitts and J. N. Pitts, *Chemistry of the Upper and Lower Atmosphere: Theory, Experiments, and Applications*, Academic Press, San Diego–London, 2000.

3 C. A. Pope, III, R. T. Burnett, M. J. Thun, E. E. Calle, D. Krewski, K. Ito and G. D. Thurston, Lung cancer, cardiopulmonary mortality, and long-term exposure to fine particulate air pollution, *J. Am. Med. Assoc.*, 2002, **287**, 1132–1141.

 This journal is © the Owner Societies 2008

4 D. W. Dockery, C. A. Pope, 3rd, X. Xu, J. D. Spengler, J. H. Ware, M. E. Fay, B. G. Ferris, Jr and F. E. Speizer, An association between air pollution and mortality in six U.S. cities, *N. Engl. J. Med.*, 1993, **329**, 1753–1759.

5 W. J. Gauderman, G. F. Gilliland, H. Vora, E. Avol, D. Stram, R. McConnell, D. Thomas, F. Lurmann, G. Margolis Helene, B. Rappaport Edward, K. Berhane and M. Peters John, Association between air pollution and lung function growth in southern California children: results from a second cohort, *Am. J. Respir. Crit. Care Med.*, 2000, **166**, 76–84.

6 J. H. Seinfeld and S. N. Pandis, *Atmospheric Chemistry and Physics: From Air Pollution to Climate Change*, Wiley Interscience, 1998.

7 H. -J. Lim and B. J. Turpin, Origins of Primary and Secondary Organic Aerosol in Atlanta: Results of Time-Resolved Measurements during the Atlanta Supersite Experiment, *Environ. Sci. Technol.*, 2002, **36**, 4489–4496.

8 C. Alves, A. Carvalho and C. Pio, Mass balance of organic carbon fractions in atmospheric aerosols, *J. Geophys. Res., [Atmos.]*, 2002, **107**(D21), 8345, DOI: 10.1029/2001JD000616.

9 R. A. Duce, V. A. Mohnen, P. R. Zimmerman, D. Grosjean, W. Cautreels, R. Chatfield, R. Jaenicke, J. A. Ogren, E. D. Pellizzari and G. T. Wallace, Organic material in the global troposphere, *Rev. Geophys. Space Phys.*, 1983, **21**, 921–952.

10 M. C. Jacobson, H. C. Hansson, K. J. Noone and R. J. Charlson, Organic atmospheric aerosols: review and state of the science, *Rev. Geophys.*, 2000, **38**, 267–294.

11 L. M. Hildemann, G. R. Markowski and G. R. Cass, Chemical composition of emissions from urban sources of fine organic aerosol, *Environ. Sci. Technol.*, 1991, **25**, 744–759.

12 D.-Y. Liu, R. J. Wenzel and K. A. Prather, Aerosol time-of-flight mass spectrometry during the Atlanta Supersite Experiment: 1. Measurements, *J. Geophys. Res., [Atmos.]*, 2003, **108**(D7), 8427.

13 A. M. Middlebrook, D. M. Murphy and D. S. Thomson, Observations of organic material in individual marine particles at Cape Grim during the First Aerosol Characterization Experiment (ACE 1), *J. Geophys. Res., [Atmos.]*, 1998, **103**, 16475–16483.

14 M. Mochida, Y. Kitamori, K. Kawamura, Y. Nojiri and K. Suzuki, Fatty acids in the marine atmosphere: factors governing their concentrations and evaluation of organic films on sea-salt particles, *J. Geophys. Res., [Atmos.]*, 2002, **107**(D17), 4325.

15 D. M. Murphy, D. S. Thomson and M. J. Mahoney, *In situ* measurements of organics, meteoritic material, mercury, and otherelements in aerosols at 5 to 19 kilometers, *Science*, 1998, **282**, 1664–1669.

16 F. Raes, T. Bates, F. McGovern and M. Van Liedekerke, The 2nd Aerosol Characterization Experiment (ACE-2): general overview and main results, *Tellus B*, 2000, **52B**, 111–125.

17 B. Warscheid and T. Hoffmann, Direct analysis of highly oxidised organic aerosol constituents by on-line ion trap mass spectrometry in the negative-ion mode, *Rapid Commun. Mass Spectrom.*, 2002, **16**, 496–504.

18 B. Warscheid, U. Kueckelmann and T. Hoffmann, Direct Quantitative Analysis of Organic Compounds in the Gas and Particle Phase Using a Modified Atmospheric Pressure Chemical Ionization Source in Combination with Ion Trap Mass Spectrometry, *Anal. Chem.*, 2003, **75**, 1410–1417.

19 A. Reinhardt, C. Emmenegger, B. Gerrits, C. Panse, J. Dommen, U. Baltensperger, R. Zenobi and M. Kalberer, Ultrahigh Mass Resolution and Accurate Mass Measurements as a Tool To Characterize Oligomers in Secondary Organic Aerosols, *Anal. Chem.*, 2007, **79**, 4074–4082.

20 M. P. Tolocka, M. Jang, J. M. Ginter, F. J. Cox, R. M. Kamens and M. V. Johnston, Formation of Oligomers in Secondary Organic Aerosol, *Environ. Sci. Technol.*, 2004, **38**, 1428–1434.

21 M. Kalberer, D. Paulsen, M. Sax, M. Steinbacher, J. Dommen, A. S. H. Prevot, R. Fisseha, E. Weingartner, V. Frankevich, R. Zenobi and U. Baltensperger, Identification of polymers as major components of atmospheric organic aerosols, *Science*, 2004, **303**, 1659–1662.

22 A. Guenther, C. N. Hewitt, D. Erickson, R. Fall, C. Geron, T. Graedel, P. Harley, L. Klinger and M. Lerdau *et al.*, A global model of natural volatile organic compound emissions, *J. Geophys. Res., [Atmos.]*, 1995, **100**, 8873–8892.

23 F. W. Went, Blue Hazes in the Atmosphere, *Nature*, 1960, **187**, 641–643.

24 S. Leungsakul, M. Jaoui and R. M. Kamens, Kinetic Mechanism for Predicting Secondary Organic Aerosol Formation from the Reaction of d-Limonene with Ozone, *Environ. Sci. Technol.*, 2005, **39**, 9583–9594.

25 D. Grosjean, E. L. Williams, II, E. Grosjean, J. M. Andino and J. H. Seinfeld, Atmospheric oxidation of biogenic hydrocarbons: reaction of ozone with b-pinene, D-limonene and *trans*-caryophyllene, *Environ. Sci. Technol.*, 1993, **27**, 2754–2758.

26 A. W. Norgaard, J. K. Nojgaard, K. Larsen, S. Sporring, C. K. Wilkins, P. A. Clausen and P. Wolkoff, Secondary limonene endo-ozonide: a major product from gas-phase ozonolysis of R -(+)-limonene at ambient temperature, *Atmos. Environ.*, 2006, **40**, 3460–3466.

27 E. J. Feltham, M. J. Almond, G. Marston, V. P. Ly and K. S. Wiltshire, Reactions of alkenes with ozone in the gas phase: a matrix-isolation study of secondary ozonides and carbonyl-containing reaction products, *Spectrochim. Acta, Part A*, 2000, **56**, 2605–2616.

28 K. Griesbaum, M. Hilss and J. Bosch, Ozonides of mono-, bi- and tricyclic terpenes, *Tetrahedron*, 1996, **52**, 14813–14826.

29 T. Hoffmann, J. R. Odum, F. Bowman, D. Collins, D. Klockow, R. C. Flagan and J. H. Seinfeld, Formation of organic aerosols from the oxidation of biogenic hydrocarbons, *J. Atmos. Chem.*, 1997, **26**, 189–222.

30 A. C. Rohr, C. J. Weschler, P. Koutrakis and J. D. Spengler, Generation and quantification of ultrafine particles through terpene/ozone reaction in a chamber setting, *Aerosol Sci. Technol.*, 2003, **37**, 65–78.

31 B. Bonn, G. Schuster and G. K. Moortgat, Influence of Water Vapor on the Process of New Particle Formation during Monoterpene Ozonolysis, *J. Phys. Chem. A*, 2002, **106**, 2869–2881.

32 S. M. Jonsson, M. Hallquist and E. Ljungstroem, Impact of Humidity on the Ozone Initiated Oxidation of Limonene, D3-Carene, and a-Pinene, *Environ. Sci. Technol.*, 2006, **40**, 188–194.

33 J. Zhang, K. E. Huff Hartz, S. N. Pandis and N. M. Donahue, Secondary Organic Aerosol Formation from Limonene Ozonolysis: Homogeneous and Heterogeneous Influences as a Function of NO_x, *J. Phys. Chem. A*, 2006, **110**, 11053–11063.

34 K. S. Docherty, W. Wu, Y. B. Lim and P. J. Ziemann, Contributions of Organic Peroxides to Secondary Aerosol Formed from Reactions of Monoterpenes with O3, *Environ. Sci. Technol.*, 2005, **39**, 4049–4059.

35 T. M. van Reken, N. L. Ng, R. C. Flagan and J. H. Seinfeld, Cloud condensation nucleus activation properties of biogenic secondary organic aerosol, *J. Geophys. Res., [Atmos.]*, 2005, **110**, DOI: 10.1029/2004JD005465.

36 Y. Iinuma, O. Boege, Y. Miao, B. Sierau, T. Gnauk and H. Herrmann, Laboratory studies on secondary organic aerosol formation from terpenes, *Faraday Discuss.*, 2005, **130**, 279–294.

37 S. Gao, M. Keywood, N. L. Ng, J. Surratt, V. Varutbangkul, R. Bahreini, R. C. Flagan and J. H. Seinfeld, Low-Molecular-Weight and Oligomeric Components in Secondary Organic Aerosol from the Ozonolysis of Cycloalkenes and a-Pinene, *J. Phys. Chem. A*, 2004, **108**, 10147–10164.

38 S. Gao, N. L. Ng, M. Keywood, V. Varutbangkul, R. Bahreini, A. Nenes, J. He, K. Y. Yoo, J. L. Beauchamp, R. P. Hodyss, R. C. Flagan and J. H. Seinfeld, Particle phase acidity and oligomer formation in secondary organic aerosol, *Environ. Sci. Technol.*, 2004, **38**, 6582–6589.

39 J. D. Surratt, S. M. Murphy, J. H. Kroll, N. L. Ng, L. Hildebrandt, A. Sorooshian, R. Szmigielski, R. Vermeylen, W. Maenhaut, M. Claeys, R. C. Flagan and J. H. Seinfeld, Chemical Composition of Secondary Organic Aerosol Formed from the Photooxidation of Isoprene, *J. Phys. Chem. A*, 2006, **110**, 9665–9690.

40 R. Szmigielski, J. D. Surratt, R. Vermeylen, K. Szmigielska, J. H. Kroll, N. L. Ng, S. M. Murphy, A. Sorooshian, J. H. Seinfeld and M. Claeys, Characterization of 2-methylglyceric acid oligomers in secondary organic aerosol formed from the photooxidation of isoprene using trimethylsilylation and gas chromatography/ion trap mass spectrometry, *J. Mass Spectrom.*, 2007, **42**, 101–116.

41 M. Mochida, Y. Katrib, J. T. Jayne, D. R. Worsnop and S. T. Martin, The relative importance of competing pathways for the

formation of high-molecular-weight peroxides in the ozonolysis of organic aerosol particles, *Atmos. Chem. Phys.*, 2007, **6**, 4851–4866.
42 D. S. Gross, M. E. Gaelli, M. Kalberer, A. S. H. Prevot, J. Dommen, M. R. Alfarra, J. Duplissy, K. Gaeggeler, A. Gascho, A. Metzger and U. Baltensperger, Real-Time Measurement of Oligomeric Species in Secondary Organic Aerosol with the Aerosol Time-of-Flight Mass Spectrometer, *Anal. Chem.*, 2006, **78**, 2130–2137.
43 D. Poppendieck, H. Hubbard, M. Ward, C. Weschler and R. L. Corsi, Ozone reactions with indoor materials during building disinfection, *Atmos. Environ.*, 2007, **41**, 3166–3176.
44 W. W. Nazaroff and C. J. Weschler, Cleaning products and air fresheners: exposure to primary and secondary air pollutants, *Atmos. Environ.*, 2004, **38**, 2841–2865.
45 Z. Fan, P. Lioy, C. Weschler, N. Fiedler, H. Kipen and J. Zhang, Ozone-Initiated Reactions with Mixtures of Volatile Organic Compounds under Simulated Indoor Conditions, *Environ. Sci. Technol.*, 2003, **37**, 1811–1821.
46 C. J. Weschler and H. C. Shields, Indoor ozone/terpene reactions as a source of indoor particles, *Atmos. Environ.*, 1999, **33**, 2301–2312.
47 X. Liu, M. Mason, K. Krebs and L. Sparks, Full-Scale Chamber Investigation and Simulation of Air Freshener Emissions in the Presence of Ozone, *Environ. Sci. Technol.*, 2004, **38**, 2802–2812.
48 A. Alshawa, A. R. Russell and S. A. Nizkorodov, Kinetic Analysis of Competition between Aerosol Particle Removal and Generation by Ionization Air Purifiers, *Environ. Sci. Technol.*, 2007, **41**, 2498–2504.
49 J. K. Nojgaard, K. B. Christensen and P. Wolkoff, The effect on human eye blink frequency of exposure to limonene oxidation products and methacrolein, *Toxicol. Lett.*, 2005, **156**, 241–251.
50 P. Wolkoff, P. A. Clausen, C. K. Wilkins and G. D. Nielsen, Formation of strong airway irritants in terpene/ozone mixtures, *Indoor Air*, 2000, **10**, 82–91.
51 G. Tamas, C. J. Weschler, J. Toftum and P. O. Fanger, Influence of ozone-limonene reactions on perceived air quality, *Indoor Air*, 2006, **16**, 168–178.
52 N. Britigan, A. Alshawa and S. A. Nizkorodov, Quantification of Ozone Levels in Indoor Environments Generated by Ionic and Ozonolysis Air Purifiers, *J. Air Waste Manage. Assoc.*, 2006, **56**, 601–610.
53 M. L. Walser, J. Park, A. L. Gomez, A. R. Russell and S. A. Nizkorodov, Photochemical Aging of Secondary Organic Aerosol Particles Generated from the Oxidation of d-Limonene, *J. Phys. Chem. A*, 2007, **111**, 1907–1913.
54 E. Kendrick, Mass scale based on CH_2 = 14.0000 for high-resolution mass spectrometry of organic compounds, *Anal. Chem.*, 1963, **35**, 2146–2154.
55 A. G. Marshall and R. P. Rodgers, Petroleomics: The Next Grand Challenge for Chemical Analysis, *Acc. Chem. Res.*, 2004, **37**, 53–59.
56 C. A. Hughey, R. P. Rodgers and A. G. Marshall, Resolution of 11 000 Compositionally Distinct Components in a Single Electrospray Ionization Fourier Transform Ion Cyclotron Resonance Mass Spectrum of Crude Oil, *Anal. Chem.*, 2002, **74**, 4145–4149.
57 C. A. Hughey, C. L. Hendrickson, R. P. Rodgers, A. G. Marshall and K. Qian, Kendrick Mass Defect Spectrum: A Compact Visual Analysis for Ultrahigh-Resolution Broadband Mass Spectra, *Anal. Chem.*, 2001, **73**, 4676–4681.
58 S. Kim, R. W. Kramer and P. G. Hatcher, Graphical method for analysis of ultrahigh-resolution broadband mass spectra of natural organic matter, the Van Krevelen diagram, *Anal. Chem.*, 2003, **75**, 5336–5344.
59 R. W. Kramer, E. B. Kujawinski and P. G. Hatcher, Identification of Black Carbon Derived Structures in a Volcanic Ash Soil Humic Acid by Fourier Transform Ion Cyclotron Resonance Mass Spectrometry, *Environ. Sci. Technol.*, 2004, **38**, 3387–3395.
60 A. M. Grannas, W. C. Hockaday, P. G. Hatcher, L. G. Thompson and E. Mosley-Thompson, New revelations on the nature of organic matter in ice cores, *J. Geophys. Res., [Atmos.]*, 2006, **111**, DOI: 10.1029/2005JD006251.
61 D. W. van Krevelen, Graphical-statistical method for the study of structure and reaction processes of coal, *Fuel*, 1950, **29**, 269–284.
62 N. M. Donahue, J. E. Tischuk, B. J. Marquis and K. E. Huff Hartz, Secondary organic aerosol from limona ketone: insights into terpene ozonolysis *via* synthesis of key intermediates, *Phys. Chem. Chem. Phys.*, 2007, **9**, 2991–2998.
63 A. A. Presto and N. M. Donahue, Ozonolysis Fragment Quenching by Nitrate Formation: The Pressure Dependence of Prompt OH Radical Formation, *J. Phys. Chem. A*, 2004, **108**, 9096–9104.
64 A. R. Rickard, D. Johnson, C. D. McGill and G. Marston, OH Yields in the Gas-Phase Reactions of Ozone with Alkenes, *J. Phys. Chem. A*, 1999, **103**, 7656–7664.
65 S. E. Paulson, M. Chung, A. D. Sen and G. Orzechowska, Measurement of OH radical formation from the reaction of ozone with several biogenic alkenes, *J. Geophys. Res., [Atmos.]*, 1998, **103**, 25533–25539.
66 *Transport and Chemical Transformation of Pollutants in the Troposphere, Volume 3: Chemical Processes in Atmospheric Oxidation; Laboratory Studies of Chemistry to Tropospheric Ozone*, ed. G. Le Bras, Springer, Berlin–Heidelberg–New York, 1997.
67 J. J. Orlando, G. S. Tyndall and T. J. Wallington, The Atmospheric Chemistry of Alkoxy Radicals, *Chem. Rev.*, 2003, **103**, 4657–4689.
68 R. Atkinson and W. P. L. Carter, Kinetics and mechanisms of the gas-phase reactions of ozone with organic compounds under atmospheric conditions, *Chem. Rev.*, 1984, **84**, 437–470.

 This journal is © the Owner Societies 2008